

Article

An Assessment of High-Density UAV Point Clouds for the Measurement of Young Forestry Trials

Robin J. L. Hartley ^{1,*} , Ellen Mae Leonardo ¹, Peter Massam ¹, Michael S. Watt ², Honey Jane Estarija ¹, Liam Wright ¹, Nathanael Melia ^{1,3} and Grant D. Pearse ¹

¹ Scion, 49 Sala Street, Private Bag 3020, Rotorua 3046, New Zealand; ellen-mae.leonardo@scionresearch.com (E.M.L.); peter.massam@scionresearch.com (P.M.); honey.estarija@scionresearch.com (H.J.E.); liam.wright@scionresearch.com (L.W.); nathanael.melia@vuw.ac.nz (N.M.); grant.pearse@scionresearch.com (G.D.P.)

² Scion, P.O. Box 29237, Fendalton, Christchurch 8041, New Zealand; Michael.Watt@scionresearch.com

³ School of Geography, Environment and Earth Sciences, Victoria University of Wellington, Kelburn, Wellington 6012, New Zealand

* Correspondence: robin.hartley@scionresearch.com

Received: 10 November 2020; Accepted: 7 December 2020; Published: 10 December 2020



Abstract: The measurement of forestry trials is a costly and time-consuming process. Over the past few years, unmanned aerial vehicles (UAVs) have provided some significant developments that could improve cost and time efficiencies. However, little research has examined the accuracies of these technologies for measuring young trees. This study compared the data captured by a UAV laser scanning system (ULS), and UAV structure from motion photogrammetry (SfM), with traditional field-measured heights in a series of forestry trials in the central North Island of New Zealand. Data were captured from UAVs, and then processed into point clouds, from which heights were derived and compared to field measurements. The results show that predictions from both ULS and SfM were very strongly correlated to tree heights ($R^2 = 0.99$, RMSE = 5.91%, and $R^2 = 0.94$, RMSE = 18.5%, respectively) but that the height underprediction was markedly lower for ULS than SfM (Mean Bias Error = 0.05 vs. 0.38 m). Integration of a ULS DTM to the SfM made a minor improvement in precision ($R^2 = 0.95$, RMSE = 16.5%). Through plotting error against tree height, we identified a minimum threshold of 1 m, under which the accuracy of height measurements using ULS and SfM significantly declines. Our results show that SfM and ULS data collected from UAV remote sensing can be used to accurately measure height in young forestry trials. It is hoped that this study will give foresters and tree breeders the confidence to start to operationalise this technology for monitoring trials.

Keywords: UAV; forestry trials; ULS; structure-from-motion; lidar; small trees; tree height

1. Introduction

Forestry trials are established to evaluate and monitor a variety of factors that affect growth. Typical examples include genetics trials, in which different provenances, families and individuals are assessed for their growth characteristics [1] or silvicultural trials, in which various silvicultural regimes are assessed to ascertain optimum management prescriptions to inform future establishment. As trials often require regular measurement of individual trees, this is a costly, time consuming, and frequently difficult task.

The use of remotely sensed data has considerable potential for overcoming difficulties associated with trial measurement. This type of data has been captured and utilised in forestry from manned aircraft since the 1920s, when aerial photography was first used in Canada [2], and satellites since

Landsat imagery was first used in 1972 [3]. Lidar, or airborne laser scanning (ALS), in particular, has emerged as a common tool for forest inventory. This technology has been widely researched for forestry since 1976 and deployed operationally for forest inventory over the past two decades [4–7].

ALS is an active remote sensing technology that emits laser pulses and then senses the backscatter of a laser's energy off a target, calculating the distance between the target and the sensor [8]. This "return" is then stored as an XYZ position relative to a specified coordinate system, known as a "point". Over a single flight, thousands of these points are collected and later reconstructed into a three-dimensional (3D) model of the area of interest, known as a point cloud. Unlike passive sensors, such as aerial photography that only sense ambient light levels, the active pulse of ALS allows for penetration of the forest canopy down to the forest floor, opening up possibilities for the measurement of forest attributes, including canopy height, canopy structure and terrain properties.

A large body of research has focussed on the application of ALS to forestry. ALS is well suited for inventory [9–14], and for predicting metrics such as height [11,15–17], diameter at breast height (DBH) [18–20], tree crown diameter and volume [21,22], leaf area index (LAI) [23–25] and stand density (for reviews, see Kaartinen et al. [26] and Eysn et al. [27]). This technology has also been used for silvicultural operations, such as identifying the optimal time for thinning, assessment of thinning intensity [28,29], and forest fuel assessment for fire modelling [30–33]. ALS has also been widely researched for carbon inventory purposes, including the estimation of above-ground biomass [34–38] and for mapping forest carbon [39–41].

Amongst inventory attributes, ALS typically estimates tree height with the highest precision [11,16] and errors are comparable to those of field measurements in tall trees [42]. The accurate estimation of height from ALS is important from an inventory perspective as this attribute is most time consuming to measure and as a result, traditional methods often rely on some form of subsampling [43]. Height can be derived from ALS using an area-based approach (ABA), where predictions are averaged to the resolution of the plot [44,45] or at individual tree level using individual tree detection (ITD) approaches [38,46].

The use of ALS within forestry is often restricted by the cost of capture. Certain operations, such as the capture of data immediately following various forestry operations for quality control purposes or inventory of small woodlots, are often too expensive to justify the cost. With the emergence of commercially available unmanned aerial vehicles (UAVs), and the miniaturization of airborne laser scanners, the expense of lidar capture has been reduced. UAV laser scanning (ULS) can be used to capture lidar in a timely and cost-effective manner over smaller areas where ALS is not cost-effective.

Compared to ALS captures that are typically collected at pulse densities of between 4 and 20 ppm², ULS can achieve far higher pulse density that can reach up to 11,000 ppm² [47]. These increases in point density significantly improve rates of tree detection using ITD [48] and may be critical for height estimation of recently planted trees with a small crown area due to a higher probability of laser interception with the apex.

There is a discrete but growing body of research into the use of ULS for the description of forest height. Early research by Jaakkola et al. [49] demonstrated that a UAV-mounted laser scanning system could predict tree height with a bias of 0.15 m, and DBH with a bias of 0.02 m from point clouds with densities ranging from 100 ppm² to 1500 ppm². Using an octocopter-based system with an Ibeo Lux scanner, Wallace et al. [50] achieved a similarly high level of accuracy (RMSE = 0.52 m (6.8%)).

Later studies confirmed the accurate prediction of height using UAVs equipped with laser scanners adapted from assisted and autonomous vehicle applications such as the Velodyne Puck series (Velodyne, San Jose, CA, USA) [51,52] and Velodyne HDL-32E [53,54] that typically collect lidar at point densities ranging from 11.5 to 800 ppm² [52,55]. More recently, specialised UAV laser scanners such as the Riegl VUX series have become available. The Riegl VUX sensors are capable of collecting point clouds at very high densities, with reported averages of 4059 ppm² [56] and 11,000 ppm² [47]. Studies using Riegl scanners have found very strong correlations between the ULS and field-measured data [47,56]. Despite these promising results, we are unaware of any published research that has explored the lower

limit at which height predictions can be robustly made using ULS, and the minimum tree height predicted to date has been 5.7 m [57].

Although costs have decreased, ULS is still cost-prohibitive for many operational uses. With low-cost, prosumer-grade UAVs becoming common, structure from motion photogrammetry (SfM) offers an appealing and cost-effective alternative to laser scanning for the assessment of key forestry metrics such as tree height. SfM photogrammetry utilises multiple overlapping images focused on an area of interest to generate a 3D representation of the area. SfM leverages computer vision and photogrammetric principles to simultaneously estimate camera position and scene geometry through common-feature mapping between overlapping images taken from different locations [58]. Through a combination of the SfM methodology and the prosumer-grade UAVs commonly used in forestry, 3D models of forest areas can be created in the form of a point cloud, which provides a low-cost alternative to lidar. SfM cannot penetrate through gaps in dense forest canopies to measure ground height to the same extent as ULS. Terrain under the canopy can only be reconstructed if there are sufficiently large gaps with adequate illumination to enable these gaps to be detected and reproduced through the SfM pipeline. With ULS, smaller gaps can be penetrated with multiple returns, meaning that partially occluded gaps can be resolved, owing to the active nature of the laser not requiring illumination. Pre-existing terrain information from other sources can be combined with SfM data if needed.

The use of photogrammetry and SfM for modelling tree attributes in forestry has been widely researched in recent years. Studies using SfM have covered a diverse range of forest environments including coniferous plantations [59–65], eucalyptus plantations [63,66], temperate coniferous forests [67–72], temperate deciduous forests [73–78], boreal forests [79–81], tropical rainforests [82], urban trees [83,84] and palm plantations [85,86]. Using SfM data, height has been accurately predicted for both large [60,71,87] and smaller trees [59,63,88]. Although the height of trees as small as 0.9 m have been predicted using SfM [63], we are unaware of any research that has investigated whether predictive accuracy deteriorates below this height.

A number of studies have compared SfM to ALS [74,75,78,89], and of these, a few have compared the precision of height predictions between ULS and SfM [51,53,54,90]. However, studies comparing the two technologies have returned conflicting results. Cao et al. [51] and Wallace et al. [90] found that ULS outperformed SfM when used to predict Lorey's Mean Height and individual tree height. In contrast, SfM was found to outperform ULS for prediction of plot-level [53] and individual tree heights [54].

In this study, six large trials of the widely grown plantation species *Pinus radiata* D. Don, that covered a height range of 0.4–6.1 m, were measured and scanned using SfM and ULS. The *P. radiata* established in these trials included a common commercial seedlot, a selection of clonal stock and a *P. radiata* × *P. attenuata* hybrid; the hybrid was also sourced through clonal propagation. Using these data, our objectives were to (i) compare the precision and bias of height models derived from ULS and SfM data, (ii) determine if a model that combines SfM data with a ULS DTM significantly improves tree height estimation over the use of only SfM data and (iii) identify height thresholds above which these data sources can be used to accurately predict tree height.

2. Materials and Methods

2.1. Data Collection

2.1.1. Study Sites and Field Data

Data were collected from four field trial sites within the central North Island of New Zealand (Figure 1) that covered a broad range of environments to test the generality of the developed methods. Topography at these four sites ranged from flat (Scion), to gently rolling (Rangipo; Kaingaroa 127) and rolling (Kaingaroa 861) terrain. Varying levels of debris and weed cover were also represented through the sites, from regularly mowed research trials (Scion) and first-rotation sites with little harvest residue

or weed cover (Rangipo) to multiple-rotation forest sites with moderate levels of harvest residue that are more typical of production forestry (Kaingaroa sites). The establishment techniques at each of the sites also differed. The Scion site was established directly into mowed, flat grass. The Rangipo site was established on a first rotation site with half of the site rip-mounded, with the other half planted into bare pasture. The two Kaingaroa sites were mechanically spot-mounded, a process by which harvest residue is cleared from the planting area and stacked in windrows, and the seedlings are established on a small mound of earth [91,92].

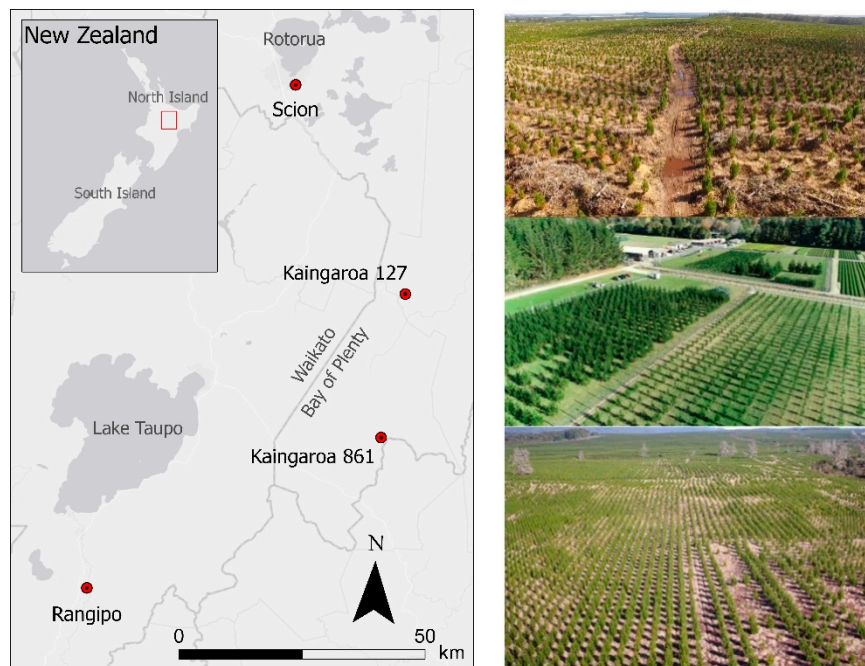


Figure 1. Map showing the location of the four study sites across the North Island of New Zealand, and aerial images demonstrating the variable site conditions—Top: Kaingaroa 861; Middle: Scion; Bottom: Rangipo.

Within three of the sites (Rangipo, Kaingaroa 127 and Kaingaroa 861) a single trial was selected, while within the Scion site we selected three trials with different age classes (Scion: North, South and West). These six trials encompassed a variety of age classes and a wide range of tree heights. At the time of UAV data capture, the age of the stands at the Scion site ranged from 5 months at the west site to 3.5 years at the south site (Table 1). The other three trials (Rangipo, Kaingaroa 127 and Kaingaroa 861) were around 3 years old at the time of capture (Table 1). There was a maximum difference of eight weeks between field measurements and UAV data capture and measurements were made in winter to mitigate the impact of this interval on height growth.

Tree heights were measured at the Kaingaroa and Rangipo sites using a height pole for trees up to ~6m tall, and a Vertex 4 hypsometer (Haglöf, Langsele, Sweden) for taller trees. Within the Scion site, a height pole was used for the smaller trees at the West site, while a Vertex was used to measure trees at the North and South sites. A total of 6616 trees were measured across the six sites with heights that ranged from 0.12 to 6.1 m (Table 2) and a mean height of 2.6 m. The distribution of measured heights was bimodal with peaks evident at both 0.4 m and 3.0 m (Figure 2).

Table 1. Description of the establishment date, point cloud capture date and age at the capture date. The number of trees (N) measured at each site and the mean and range of measured heights are also shown.

Site	Trial Age and Capture Date			Number of Trees and Height Statistics			
	Estab.	Capture	Age at	N	Min.	Mean	Max.
	Date	Date	Capture (Yrs)		m	m	m
Rangipo	August 2016	July 2019	3	1940	0.6	3.3	5.6
Kaingaroa 861	August 2015	June 2018	3	1385	0.4	2.9	5.5
Kaingaroa 127	July 2016	June 2019	3	938	0.7	2.5	4.3
Scion: South	October 2015	April 2019	3.5	613	1.4	4.2	6.1
Scion: North	October 2016	April 2019	2.5	875	0.34	1.7	3.1
Scion: West	October 2019	March 2020	0.4	865	0.12	0.4	0.61
Total and mean				6616	0.12	2.6	6.1

Table 2. Unmanned aerial vehicle (UAV) flight parameters for data captures.

SfM	Altitude (m)	Overlap % (Forward:Side)	Point Density (pt/m ²)	Speed (m/s)	GSD (cm/pxl)
Rangipo	74	90:80	580	3.5	1.9
Kaingaroa 861	74	90:80	443	3.5	1.9
Kaingaroa 127	74	90:80	573	3.5	1.9
Scion: North and South	60	85:80	939	3	1.6
Scion: West	74	90:80	410	3.5	2.0
ULS	Altitude (m)	Line Spacing (m)	Point Density (pt/m ²)	Speed (m/s)	
Rangipo	45	16	638	5	
Kaingaroa 861	45	16	649	5	
Kaingaroa 127	45	16	631	5	
Scion: North and South	45	21	325	5	
Scion: West	45	10	487	5	

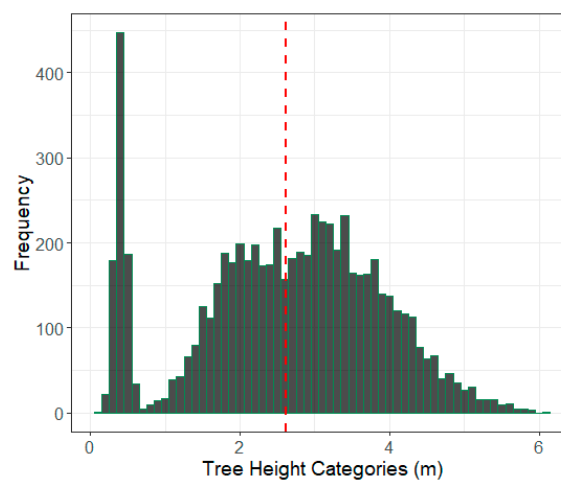


Figure 2. Distribution of tree heights across all four study sites binned at 0.1 m intervals. The red dashed line has been drawn at the mean tree height of all trees in the study (2.6 m).

2.1.2. UAV Data Acquisition Methodology

Ground control was set up prior to data capture. A Trimble Geo7X handheld GPS unit (Trimble Inc., Sunnyvale, CA, USA) with a Trimble Zephyr Model 2 external aerial was used to survey in a minimum of five ground control points (GCPs) following best practice guidelines for Pix4D [93]. RMSE of GCPs collected per site ranged from 0.01 m to 0.11 m.

ULS data were captured using a LidarUSA Snoopy V-series system (Fagerman Technologies, INC., Somerville, AL, USA), with an integrated Riegl MiniVUX-1 UAV scanner (Riegl, Horn, Austria),

mounted on a DJI Matrice 600 Pro UAV (DJI Ltd., Shenzhen, China). SfM data was captured using a DJI Phantom 4 Pro UAV (DJI Ltd., Shenzhen, China) equipped with an integrated 1-inch 20 MP RGB camera.

The UgCS software (SPH Engineering, Riga, Latvia) was used for ULS data capture as this software can incorporate adaptive banking turns into flight plans, reducing the potential error in the scanner's IMU position during turns. Map Pilot (Drones Made Easy, San Diego, CA, USA) was used for photogrammetry and was selected for its terrain-following functionality that ensured an even GSD across images. The altitude, line spacing and speed required to obtain a range in point density of 325–649 pt/m² between the sites are specified in Table 2.

Flight parameters for SfM broadly followed guidelines from Dandois et al. [75] who stipulate that flights should only be carried out under clear sky conditions with wind speeds of less than 20 km/h and high solar angle to reduce the effects of shadow. A flight altitude of approximately 80 m AGL (74 m was chosen to obtain a GSD of approximately 2 cm), and at least 80% forward overlap are also stipulated in the same study. We increased our overlap in line with guidance from Frey et al. [61], who recommended higher forward overlap as being optimal for the reconstruction of more complex forest environments. Flight parameters for the Scion North and South datasets were slightly different as these data were captured as part of a previous experiment [94]. The default camera settings were used with the Map Pilot application, which included infinity focus, auto exposure and a nadir camera angle. The only changes made to the default was to set white balance to “sunny”. With these settings, the aperture, shutter speed and ISO were variable and controlled by the application. The point density of the SfM captures ranged from 410 to 939 pt/m² (Table 2).

2.2. Data Processing and Analysis

The methodology for this project involved three broad phases: (1) processing of raw data into point clouds, (2) quality control and cleaning of the point cloud data, and (3) analysis of the point cloud data.

2.2.1. Processing Raw Data

UAV Laser Scanning

ULS data generally have to be retrieved from the scanner in the manufacturer's native format and then processed into a more universal format, such as LAS or ASCII. The Snoopy V-Series can be operated as a PPK (post-processed kinematic) system, meaning that raw sensor data from the scanner can be post-processed with reference to GNSS base station data to increase the inherent accuracy of the point cloud. The system uses the Inertial Explorer Xpress (IE Xpress) (NovAtel Inc., Calgary, AB, Canada) software suite to apply a correction to the GNSS rover trajectory data from the GNSS log data captured by the CHCX900B base station (CHC Navigation, Shanghai, China) during the flight operations. ScanLook Point Cloud Export (Scanlook PC) (Fagerman Technologies INC., Somerville, AL, USA) was then used to combine the post-processed trajectory data with the raw sensor data. This data can then be exported in a universal point cloud format (in this case LAS). ULS data collected per site has a maximum RMSE of 0.01 m for horizontal values and 0.03 m for elevation values.

Rudimentary filtering was carried out on the raw lidar data within Scanlook PC. Further de-noising of the point cloud was carried out in LasTools (see Section 2.2.2). Turns and irrelevant flight lines, such as taxiing flights to and from the area of interest, were removed by a quality control process. This was carried out in the Graphics Mode feature of Scanlook PC, in which the trajectory of the flights can be filtered to remove sections of the point cloud that could provide potential sources of error. Crucially, ScanLook PC also applies boresight calibration angles and lever arm offsets. These two corrections are, respectively, the X, Y and Z offsets between the IMU and the scanner, and the X, Y and Z offsets between the IMU and the GNSS antenna and are critical measurements to ensure the accuracy of the point clouds. Failure to calibrate the data for either of these two measurements can

build inherent errors into the point cloud data, such as the mismatching of opposing flight lines, or errors in point alignment.

Structure from Motion

The software Pix4Dmapper (Pix4D, Lausanne, Switzerland), hereafter referred to as Pix4D, was used to process the raw images from the UAV and generate the required spatial outputs. Pix4D follows three basic stages during the processing of SfM data that include: 1. Initial Processing; 2. Point Cloud and Mesh generation; and 3. DSM, Orthomosaic and Index generation. For this study, the standard 3D mapping processing settings were followed within Pix4D, except for the following adjustments. For the Initial Processing stage, Geometrically Verified Matching was disabled under the advanced and the Matching Table. This is designed to discard geometrically inconsistent matches and is promoted as being useful for projects that include rows of plants in agricultural fields [95]. Initial trials with the settings returned better results for datasets in this study with this option switched off. In the Point Cloud and Mesh generation stage, the Minimum Number of Matches was increased from the standard setting of three to five, to reduce noise and improve the quality of the point cloud. Trials with the minimum number of matches indicated three to be optimal for the data. The Classify Point Cloud option was also selected to aid in the generation of a DTM. Point clouds were exported as a single merged file in LAS format. No changes were made to the settings in stage three, other than to specify that all spatial outputs other than an orthomosaic should not be produced. Once the initial processing stage was completed, spatial reference data in the form of 3D GCPs were added to the projects to reprocess the models into a spatial coordinate system that matched the lidar (NZGD2000/New Zealand Transverse Mercator 2000 (EGM 96 Geoid)). A point cloud and orthomosaic were generated in subsequent steps and exported in LAS and TIF format, respectively.

2.2.2. Point Cloud Processing

The tree locations were manually identified to eliminate the error in data matching between the predicted and measured tree tips so that the precision of the methods at predicting height could be assessed. Using ArcGIS Pro 2.5.1 [96], individual trees were manually annotated on the RGB orthomosaic that was created for each site in Pix4D using the trial tree maps as a reference. These annotations were then buffered and used to confine the search area for tree tips within the point cloud. Figure 3 shows an example of these tree annotations overlaid on a raster of predicted height.

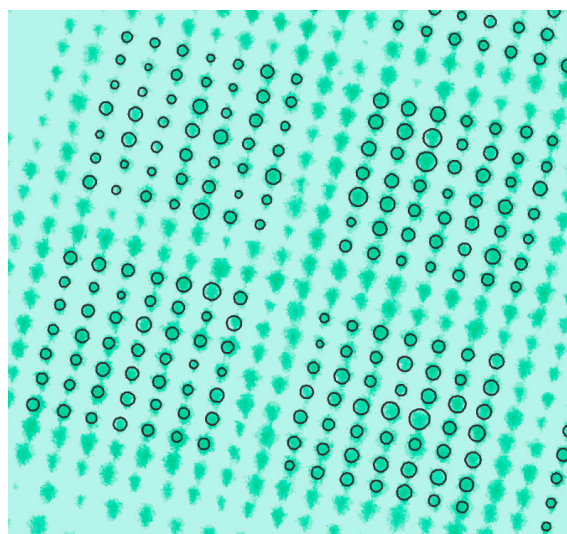


Figure 3. Image of the ULS point cloud at Rangipo overlaid with the annotations that were assigned to each tree in the trial.

In order to extract the required metrics from the ULS and SfM point clouds, it was first necessary to process the data. Using LAStools software version 190,404 [97], the point cloud datasets were tiled, de-noised and thinned. The datasets were ground classified using the lasground_new algorithm with a terrain resolution of 10 m for the Scion data and 3 m for all other datasets. The Kaingaroa datasets were processed separately with care given to ensure the ground classification accounted for the spot mounds present at these sites. The point clouds were then height normalised to the terrain model generated from the ground classified points. For the datasets combining ULS ground data with SfM data, the ULS ground terrain models at 0.5 m resolution were merged with unclassified SfM point clouds before height normalisation.

Using these individual tree annotations, the predicted heights for each tree were extracted from the normalised point cloud heights using the LidR library [98] in R statistical software version 3.6.0 [99]. Specifically, the grid_canopy algorithm was used to identify the local maxima within the individual polygons defined around each tree canopy.

2.2.3. Integrating SfM DSM with ULS DTM

In order to integrate the ULS DTM with the SfM DSM, the models were first accurately aligned within the CloudCompare software version 2.1.1 [100]. This was undertaken by utilising the “Align (point pairs picking)” tool to align the point clouds by the ground control points laid out across each site. Aligned point clouds were then exported in LAS format and analysed following the methodology outlined in 2.2.2 and these point clouds will be referred to hereafter as SfM_{UTM}.

2.3. Statistical Analysis

The precision and bias of height predictions using the three data types were assessed using the root mean square error (RMSE), mean bias error (MBE), and the coefficient of determination (R^2). These metrics were calculated using the following equations:

$$RMSE = \sqrt{\frac{\sum_{i=1}^n (\hat{y}_i - y_i)^2}{n}}$$

$$MBE = \frac{1}{n} \sum_{i=1}^n y_i - \hat{y}_i$$

$$R^2 = \frac{\sum_i (\hat{y}_i - \bar{y})^2}{\sum_i (y_i - \bar{y})^2}$$

where y_i represents field measured heights, \hat{y}_i represents predicted heights from UAV point clouds, \bar{y} is the average of the observed values and n represents the sample size. The percentage RMSE (RMSE%) was also determined through expressing the RMSE as a percentage of the average observed values, \bar{y} , as $RMSE\% = 100 (RMSE/\bar{y})$. The effect of height on error was examined using absolute error (AE) and percentage error (PE), which were both calculated at the tree level. The absolute error for each tree was determined from $|y_i - \hat{y}_i|$. The percentage error was determined for each tree from $100 \times AE/y_i$. The effect of height on error was examined through plotting values of AE and PE against tree heights categorised into 0.5 m bins ranging from 0–0.5 to 6.5–7.0 m.

3. Results

Across all sites, the results from the ULS data show a high level of precision and a low level of bias (Table 3 and Figure 4). Overall, there was a very strong correlation between ULS predictions and field-measured heights with an R^2 of 0.99 (Figure 4), and RMSE of 0.15 (5.91%) (Table 3). There was slight underprediction of height, as evidenced by the MBE of 0.05 m (Table 3), but overall there was little apparent bias in predictions across the height range (Figure 4a).

Table 3. Statistics describing the precision and bias of predictions of height using ULS, SfM and SfM that used a ULS DTM (SfM_{UTM}). Shown are the coefficient of determination, root mean square error (RMSE) and mean bias error (MBE).

Site	ULS			SfM Dataset			SfM with ULS DTM		
	R ²	RMSE	MBE	R ²	RMSE	MBE	R ²	RMSE	MBE
		m	m		m	m		m	m
Rangipo	0.97	0.15	0.06	0.87	0.56	0.48	0.88	0.47	0.38
Kaingaroa 861	0.94	0.19	0.03	0.86	0.42	0.30	0.86	0.29	0.07
Kaingaroa 127	0.94	0.17	0.06	0.79	0.53	0.44	0.81	0.53	0.45
Scion: South	0.97	0.17	0.03	0.80	0.61	0.40	0.81	0.60	0.45
Scion: North	0.95	0.11	0.00	0.76	0.37	0.31	0.75	0.27	0.18
Scion: West	0.27	0.13	0.10	0.05	0.31	0.29	0.02	0.37	0.35
Mean	0.99	0.15	0.05	0.94	0.48	0.38	0.95	0.43	0.32

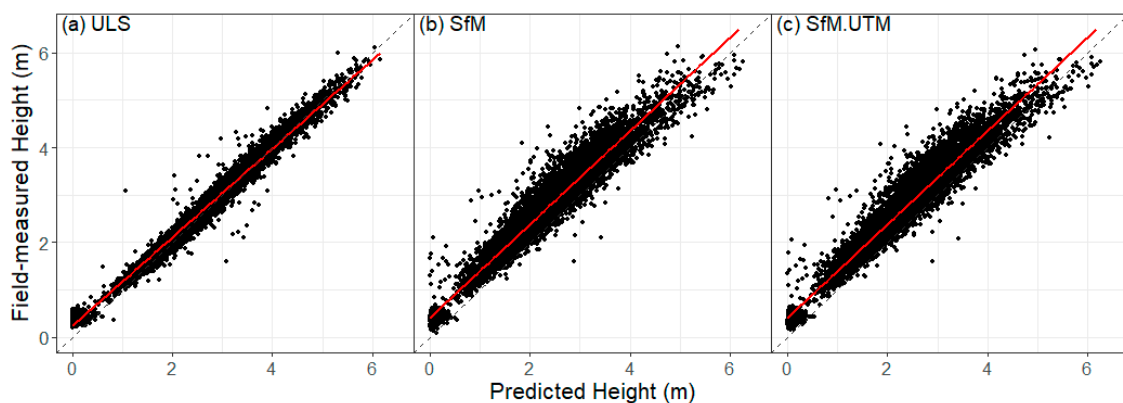


Figure 4. Correlation between field-measured tree heights and heights predicted from (a) ULS, (b) SfM and (c) SfM_{UTM}. The 1:1 line is shown as a dashed black line and a linear model fitted through the data is shown as a solid red line.

Variation in precision between individual sites was relatively low for all sites, apart from Scion West, in which the trees were markedly smaller. For the five sites with the tallest trees, the R² ranged from 0.94 to 0.97, with RMSE and RMSE%, respectively, ranging from 0.11 to 0.19 m and from 4.01 to 6.61%. Bias was relatively low for these five sites, ranging from 0 to 0.06 m, which was also evidenced by the close correspondence of predictions to the 1:1 line for these sites (Figure 5a–e). Predictions of height at the Scion West site had far lower precision (R² = 0.27, RMSE = 32.1%) and were also more biased (MBE = 0.10 m) with ULS markedly underestimating tree height (Figure 5f).

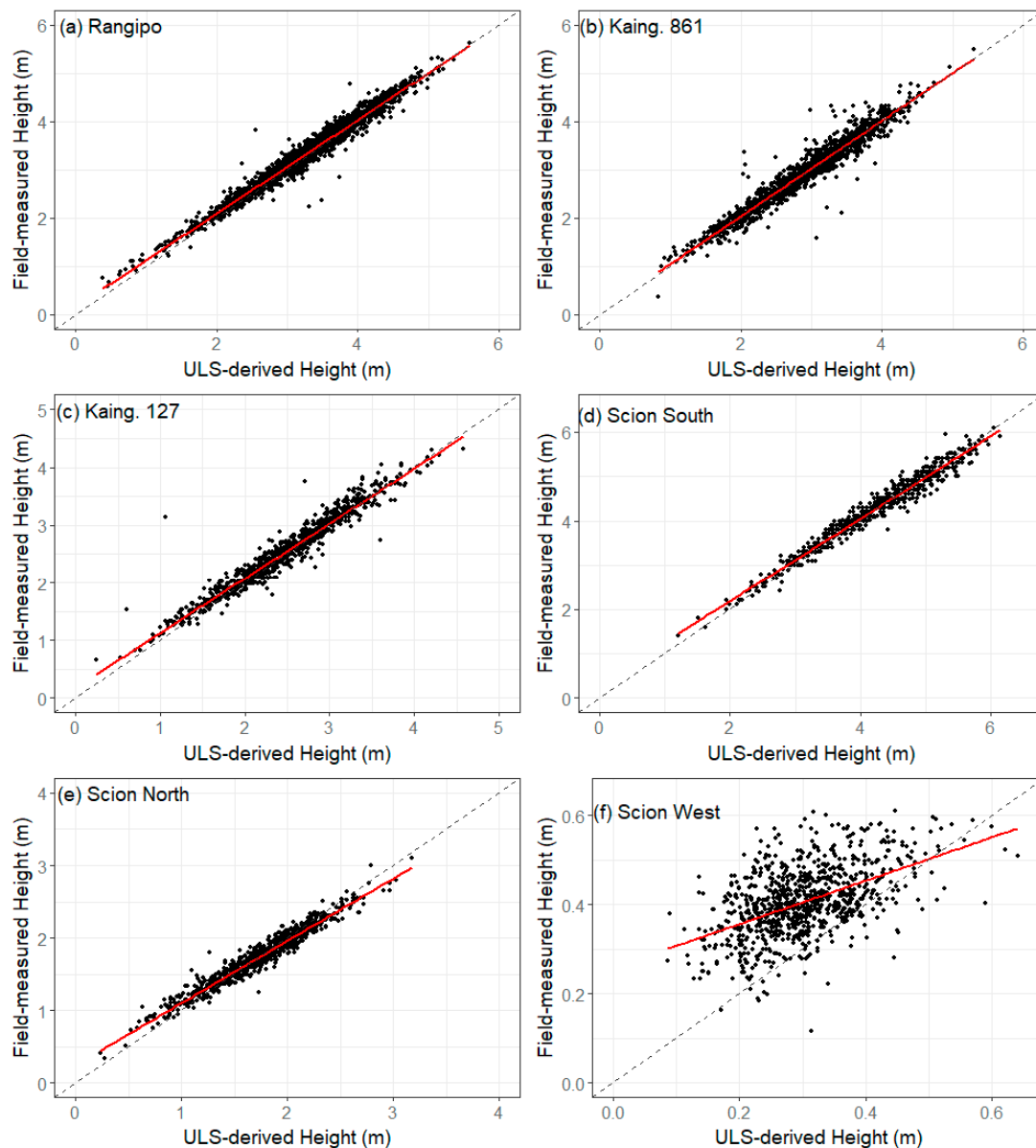


Figure 5. The relationship between field-measured and ULS-derived tree heights for (a) Rangipo, (b) Kaingaroa 861, (c) Kaingaroa 127, (d) Scion, South, (e) Scion, North and (f) Scion, West. Note the different y-axis scales between panels. The 1:1 line is shown as a dashed black line and a linear model fitted through the data is shown as a solid red line.

Predictions of height from SfM had a lower precision and greater bias than predictions using ULS (Table 3 and Figure 4b). For the dataset that combined data from all sites, the precision was moderate to high with R^2 of 0.94 and RMSE of 0.48 m (18.5%) (Table 3). Using this method, there was underprediction of height as shown by the MBE of 0.38 and this bias was also evident in Figure 4b.

There was little variation in model precision for the five sites with the tallest trees, with R^2 ranging from 0.76 to 0.87 (Table 3). However, the model precision diminished greatly for Scion West, which had an R^2 of 0.05 and RMSE of 75.9% (Table 3). At all sites, SfM underpredicted tree height (Figure 6; Table 3) with the extent of this bias greatest for Scion West (Figure 6f).

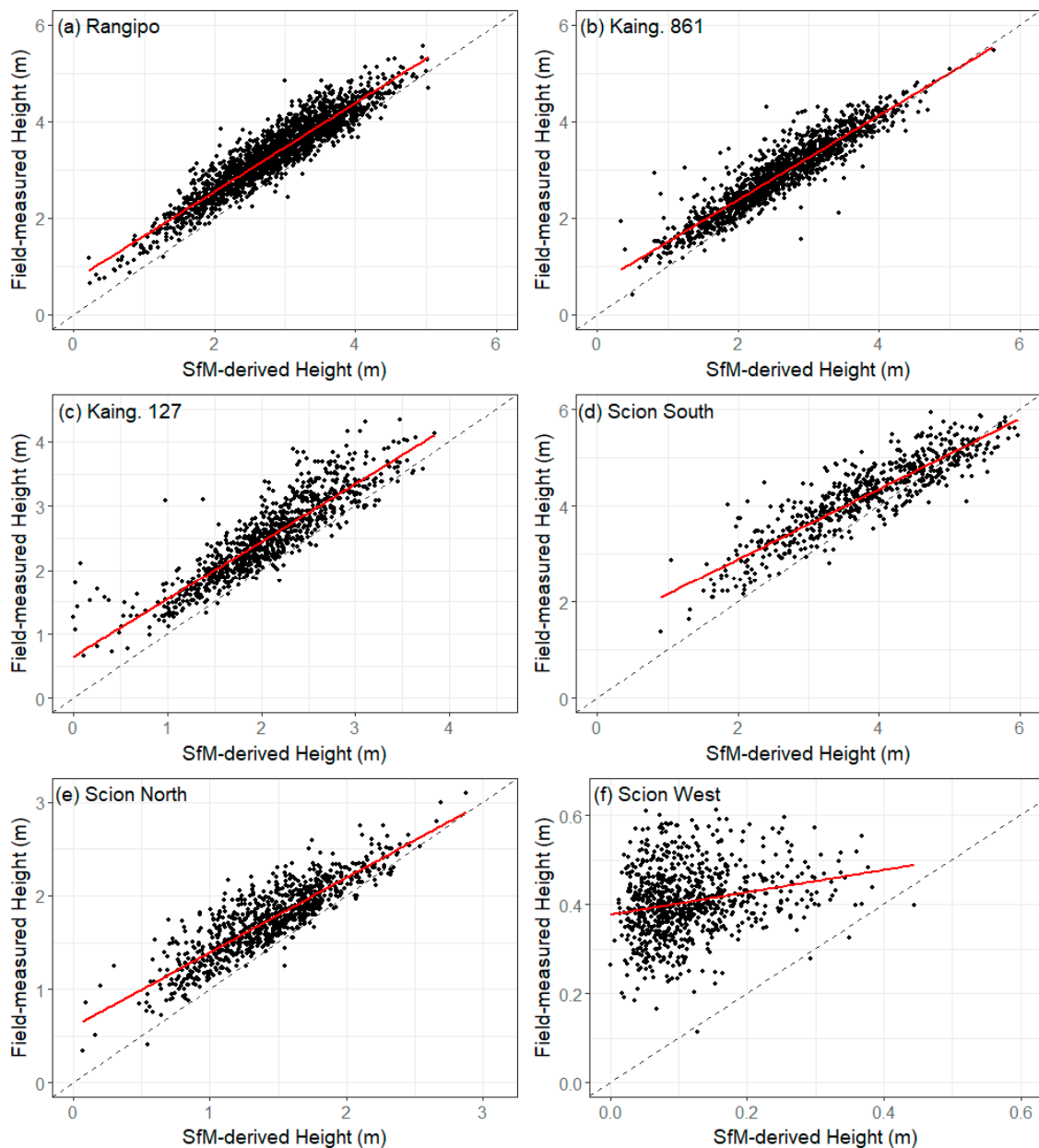


Figure 6. The relationship between field-measured and SfM-derived tree heights for (a) Rangipo, (b) Kaingaroa 861, (c) Kaingaroa 127, (d) Scion, South, (e) Scion, North and (f) Scion, West. Note the different y-axis scales between panels. The 1:1 line is shown as a dashed black line and a linear model fitted through the data is shown as a solid red line.

Compared to the use of SfM data alone, there were slight gains in precision and bias when SfM_{UTM} was used to predict height (Table 3). Using the SfM_{UTM} dataset, predictions across all sites had an R^2 of 0.95 and RMSE of 0.43 m (16.5%) (Table 3). Using this method, there was underprediction of height, as shown by the MBE of 0.32, and this bias was also evident in Figure 4c.

Height predictions made using the SfM_{UTM} data showed little variation in model precision for the five sites with the tallest trees, with R^2 ranging from 0.75 to 0.88 (Table 3). Again, the model precision diminished significantly for Scion West, which had an R^2 of 0.02 and RMSE of 91.0% (Table 3). At all sites, SfM_{UTM} underpredicted tree height with the extent of this bias greatest for Scion West (Table 3).

Using the ULS dataset, pooled across all six sites, the absolute height errors declined gradually from the smallest two categories of trees to the taller trees (Figure 7a). Values of the percentage error declined sharply from 87.2% and 63.7%, respectively, for the 0–0.5 and 0.5–1.0 m categories to 8.1% for

trees that had a height of 1–1.5 m (Figure 7c). The percentage error reached a minimum of 0.9% for the tallest group with heights of 6–6.5 m (Figure 7c).

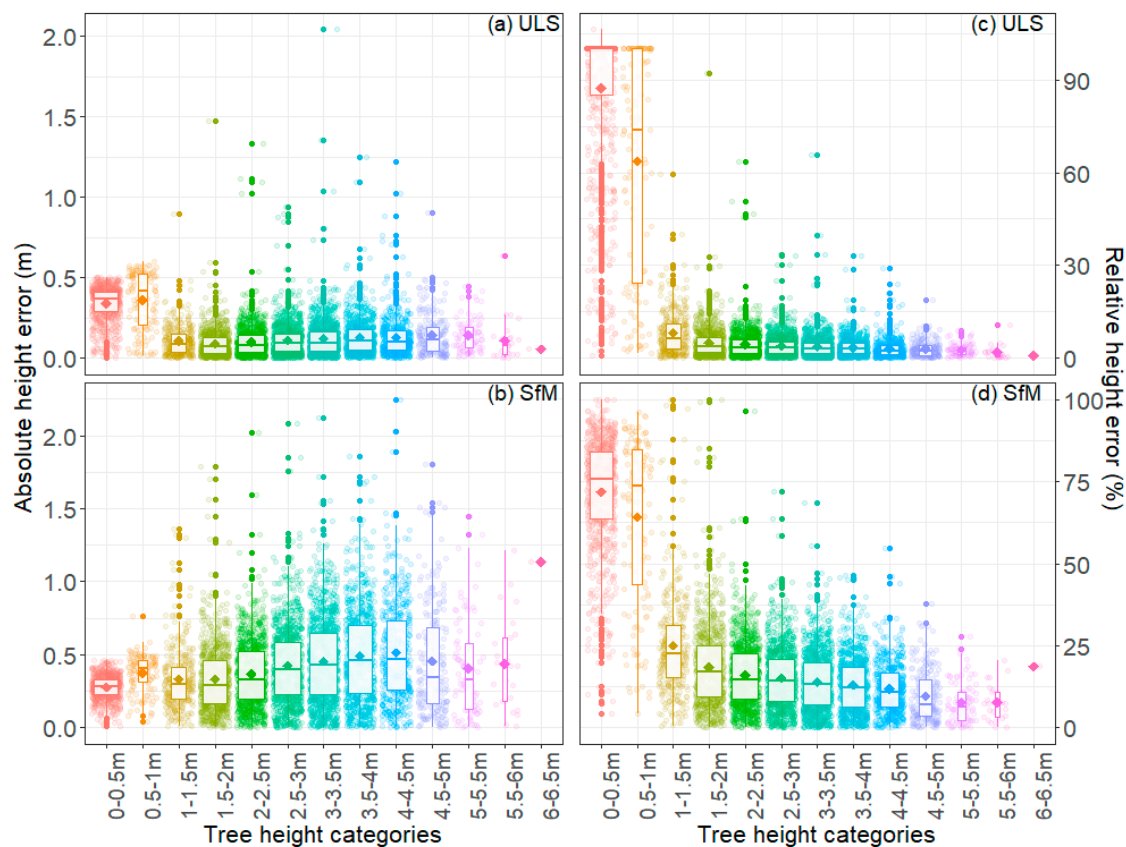


Figure 7. Variation between tree height categories in the absolute error (a,b) and percentage error (c,d) between measured values and those predicted by (a,c) ULS and (b,d) SfM. Box plots show median error for each category, along with confidence intervals. Box width represents sample size. Diamonds represent the mean error for each height class.

In contrast to ULS, there were increases in the mean absolute error of SfM predictions with increasing height (Figure 7b), with values reaching a maximum mean error of ca. 0.5 m at heights exceeding 3.5 m (Figure 7b). There were very steep reductions in percentage error from mean values of 71.7 and 64.1%, respectively, for the two smallest height categories to 25.1% for trees that were between 1 and 1.5 m (Figure 7d). More gradual reductions in percentage error occurred above this height, reaching values as low as 7.7% for trees within the 5–5.5 m and 5.5–6 m height classes.

4. Discussion

This study highlights the utility of point cloud data collected from UAVs for estimating tree height in young forestry trials. Although predictions made by ULS and SfM were both strongly related to measured height ($R^2 = 0.99$, and $R^2 = 0.94$, respectively), there was a three-fold difference in RMSE between the two methods which is a more sensitive indicator of precision (RMSE = 0.15 vs. 0.48 m). The substitution of the ULS DTM into the SfM dataset resulted in very little improvement in precision over the use of only SfM data. Tree heights that were less than 1 m could not be accurately estimated using SfM or ULS.

Our predictions of height using ULS had RMSE of 5.91%, which is consistent with previous literature. Similar levels of precision and accuracy were observed in mixed boreal forests by Jaakkola et al. [52] who reported a coefficient of determination of 0.95 and relative RMSE of 6.8% between ULS and field measurements. Wallace et al. [57] observed a relative RMSE of 6.8% when

comparing individual ULS-derived tree heights to field-measured heights in stands of *Eucalyptus globulus* Labill. Dash et al. [101] also found an equivalent level of accuracy to this study in a mature stand of *P. radiata* with an RMSE of 6.8%.

Our results show that ULS slightly underestimates tree height and that this bias is highest for the smallest trees. The underestimation of tree height is a well-documented issue for single tree and area-based predictions from lidar [102–105]. This underestimation could be attributable to inadequate pulse density, use of a beam footprint that exceeds the width of the tree canopy [106], imperfections in the algorithms used in creating the DTM, DSM and CHM, pulse penetration through the canopy to the ground, and a lack of comprehensive pulse coverage [8]. Due to the very high pulse density, the open canopy of our study sites and efforts to minimise error in the DTM, errors were most likely to be attributable to imperfections in the algorithms used to create, DSM or CHM but could also result from a higher angle of incidence of the laser pulse or a larger beam footprint.

In our results, we observed a higher level of error in tree height accuracy (RMSE = 0.15 m at 45 m) than the reported accuracy of the MiniVUX-1UAV scanner (0.015 m at 50 m range, under Riegl test conditions [107]). Liang et al. [47], linked this to the influence of greater beam divergence under field conditions having a negative effect on positioning accuracy of points. A large footprint size, attributable to greater beam divergence, has been attributed to the creation of random error in the point cloud through differences in the incidence angle [52]. With an increased angle of incidence from the nadir, the beam footprint increases and, therefore, the strength of the return is averaged across a greater area introducing error into the point [108]. This same explanation would apply to a nadir pulse with a beam footprint wider than the target, such as a tree tip, or a small tree. The high overlap and minimal filtering of incidence angle in this study could explain some of the height error in our results. Increasing the overlap has been demonstrated to introduce error into the point cloud and could remove the benefits of the additional point coverage over the target [47]. Further work to quantify the error introduced with various angles of incidence should be carried out to establish optimal overlap settings for forestry applications.

Although predictions of height using SfM data were relatively precise, these predictions had greater bias and a lower level of accuracy than the ULS, which is consistent with previous research [51,90]. Compared to ULS, the use of SfM point clouds resulted in a threefold increase in the RMSE (0.15 vs. 0.48 m) and RMSE% (5.91 vs. 18.5%). Previous research, that has used SfM point clouds for the measurement of tree heights, demonstrates a wide range of precision between studies, with RMSE% ranging from 1.89 to 19.4% and the coefficient of determination ranging from 0.21 to 0.99 [59,60,62–65,69,71,74–78,80,83–88,109–111]. Although our overall results were at the less precise end of the RMSE% range, this was attributable to the inclusion of small trees within the study, which resulted in increases in the percentage error. When height error was expressed in absolute terms, our results are consistent with other studies that have found SfM to be capable of measuring tree heights to within 0.5 m of field-measured heights [59,62,63,65,85,88].

It is well known that SfM cannot describe the DTM as accurately as ULS [60] and the lower precision of the DTM could introduce error into tree height estimates from SfM. We tested the impacts of this factor on height predictions through integrating the actively sensed ULS DTM with the SfM data (SfM_{UTM}). The results showed a very modest increase in the correlation coefficient of 0.01 ($R^2 = 0.95$ vs. 0.94), a slight decrease in RMSE of 0.05 m (0.43 vs. 0.48 m), and a corresponding small reduction in RMSE% of 2% (16.5 vs. 18.5%). This supports previous findings [74] and is consistent with Hentz et al. [63] who hypothesised that it is possible to generate an accurate DTM from SfM when the canopy is sufficiently open. It was interesting to note that height predictions from ULS still had a significantly higher accuracy than those predicted from SfM_{UTM}, which suggests these precision gains were attributable to other factors.

Further research should be undertaken to optimise settings and parameters for SfM acquisition. In this study, the flight parameters were carefully planned to reflect findings from Dandois et al. [75] and Frey et al. [61] in order to minimise the errors caused by image overlap, wind and weather.

The camera parameters that optimise image quality in aerial photography and photogrammetry are a large sensor, a focal length of between 24 and 35 mm, and an ISO setting optimised to ensure a shutter speed fast enough to minimise motion blur [112,113]. The focal length of the Phantom 4 Pro is 8.8 mm [114], which is considerably smaller than the suggested optimal focal length. A smaller focal length will introduce a greater level of lens distortion and could cause some error in the reproduction of the point cloud [112]. The focal length of the Phantom 4 Pro is fivefold smaller than the focal length of the camera that achieved the lowest RMSE from the literature [88]. The sensor size of the Phantom 4 Pro is almost three times smaller than the camera that achieved the lowest RMSE, which would result in reduced sensitivity [88]. For future study, a direct comparison between multiple cameras is suggested, so that the effect of camera parameters on tree height measurement can be explored in greater depth.

Within this study, Pix4D was used to process point cloud data as this is one of the most widely used software programmes for this purpose [65,68,74,79,83,86,87,115]. The SfM software could potentially introduce errors in the point cloud, notably in the creation of the DTM [62]. Studies that have trialled more than one SfM software to predict tree height have found significant differences in precision [68,116] and further research is required to compare the impact of this factor on the predictive precision of tree heights. As well as the SfM process itself, a number of studies have suggested that the algorithms used to create the CHM and individual tree crown delineation could have a possible smoothing effect on the SfM heights [62,63,117]. The methodology followed in this study to analyse tree heights did not create a CHM, and the negative bias was still observed. This is an interesting finding, as it means that the CHM creation phase can be ruled out as the sole cause of the bias, although it cannot be excluded as a contributing factor.

Similarly, there are many factors involved in ULS acquisition that could be refined to improve height predictions. Error from ULS acquisition is influenced by beam divergence (and consequently beam footprint), range accuracy, maximum range and the height that the scanner is flown above the target. There is now a range of UAV laser scanners on the market, and all have different attributes that could affect the accuracy of forestry measurements [118]. The interaction between these variables has not been well studied for forestry applications, and we echo the conclusion of Liang et al. [47] that further study in this area is required to optimise data collection and predictions of key metrics such as height.

5. Conclusions

This study has shown that point cloud data acquired from a UAV can be used to accurately predict tree heights. Our results extend previous research by demonstrating that tree height can be accurately quantified down to a threshold of 1 m. Below this height, error increases significantly. Although SfM was not as accurate as ULS for prediction of tree height, this method could provide a more cost-effective alternative to ULS. Further research should be undertaken to refine collection and data processing methods for both ULS and SfM.

Author Contributions: Conceptualization, R.J.L.H., G.D.P., M.S.W., and N.M.; methodology, R.J.L.H., G.D.P., E.M.L., and N.M.; formal analysis, E.M.L. and R.J.L.H.; investigation, R.J.L.H., E.M.L., G.D.P.; data curation, R.J.L.H., P.M., L.W., and H.J.E.; writing—original draft preparation, R.J.L.H.; writing—review and editing, M.S.W., G.D.P.; visualization, R.J.L.H., E.M.L., and M.S.W.; supervision, R.J.L.H., M.S.W. and G.D.P. All authors have read and agreed to the published version of the manuscript.

Funding: This research was funded by Scion's Strategic Science Investment Funding (SSIF) provided by the Ministry of Business Innovation and Employment (MBIE). Additional co-funding was provided by the Forest Growers Levy Trust.

Acknowledgments: The authors would like to acknowledge Timberlands Ltd. and NZ Forest Managers for access to their forests for study sites. We would also like to acknowledge Toby Stovold for assisting with the UAV data capture, and the Scion Forest Systems and Plant Biotech field teams for their tremendous efforts in measuring the field trials on a regular basis. Thanks should also be given to Agnieszka Boron, Glenn Thorlby, Shideen Nathan, Alex Manig, Loretta Garrett and Simeon Smaill of Scion for their assistance with queries regarding the forestry trials and their measurement.

Conflicts of Interest: The authors declare no conflict of interest. The funders had no role in the design of the study; in the collection, analyses, or interpretation of data; in the writing of the manuscript, or in the decision to publish the results.

References

1. Costa e Silva, J.; Dutkowski, G.W.; Gilmour, A.R. Analysis of early tree height in forest genetic trials is enhanced by including a spatially correlated residual. *Can. J. For. Res.* **2001**, *31*, 1887–1893. [[CrossRef](#)]
2. Leckie, D.G. Advances in remote sensing technologies for forest surveys and management. *Can. J. For. Res.* **1990**, *20*, 464–483. [[CrossRef](#)]
3. Iverson, L.R.; Graham, R.L.; Cook, E.A. Applications of satellite remote sensing to forested ecosystems. *Landsc. Ecol.* **1989**, *3*, 131–143. [[CrossRef](#)]
4. Maclean, G.A.; Krabill, W. Gross-merchantable timber volume estimation using an airborne LIDAR system. *Can. J. Remote Sens.* **1986**, *12*, 7–18. [[CrossRef](#)]
5. Nelson, R.; Krabill, W.; Tonelli, J. Estimating forest biomass and volume using airborne laser data. *Remote Sens. Environ.* **1988**, *24*, 247–267. [[CrossRef](#)]
6. Nelson, R. How did we get here? An early history of forestry lidar. *Can. J. Remote Sens.* **2013**, *39*, S6–S17. [[CrossRef](#)]
7. Caccamo, G.; Iqbal, I.A.; Osborn, J.; Bi, H.; Arkley, K.; Melville, G.; Aurik, D.; Stone, C. Comparing yield estimates derived from LiDAR and aerial photogrammetric point-cloud data with cut-to-length harvester data in a Pinus radiata plantation in Tasmania. *Aust. For.* **2018**, *81*, 131–141. [[CrossRef](#)]
8. Gatzliolis, D.; Fried, J.S.; Monleon, V.S. Challenges to estimating tree height via LiDAR in closed-canopy forests: A parable from Western Oregon. *For. Sci.* **2010**, *56*, 139–155.
9. Hyyppä, J.; Yu, X.; Hyyppä, H.; Vastaranta, M.; Holopainen, M.; Kukko, A.; Kaartinen, H.; Jaakkola, A.; Vaaja, M.; Koskinen, J.; et al. Advances in forest inventory using airborne laser scanning. *Remote Sens.* **2012**, *4*, 1190–1207. [[CrossRef](#)]
10. Næsset, E. Airborne laser scanning as a method in operational forest inventory: Status of accuracy assessments accomplished in Scandinavia. *Scand. J. For. Res.* **2007**, *22*, 433–442. [[CrossRef](#)]
11. Watt, M.S.; Meredith, A.; Watt, P.; Gunn, A. The influence of LiDAR pulse density on the precision of inventory metrics in young unthinned Douglas-fir stands during initial and subsequent LiDAR acquisitions. *N. Z. J. For. Sci.* **2014**, *44*, 18. [[CrossRef](#)]
12. de Oliveira, L.T.; Ferreira, M.Z.; de Carvalho, L.M.T.; Filho, A.C.F.; Oliveira, T.C.A.; Silveira, E.M.O.; Junior, E.F.W.A. Determining timber volume of eucalyptus stands by airborne laser scanning. *Pesqui. Agropecu. Bras.* **2014**, *49*, 692–700. [[CrossRef](#)]
13. Hill, A.; Breschan, J.; Mandallaz, D. Accuracy assessment of timber volume maps using forest inventory data and LiDAR canopy height models. *Forests* **2014**, *5*, 2253–2275. [[CrossRef](#)]
14. Watt, M.S.; Adams, T.; Marshall, H.; Pont, D.; Lee, J.; Crawley, D.; Watt, P. Modelling variation in pinus radiata stem volume and outerwood stress-wave velocity from LiDAR metrics. *N. Z. J. For. Sci.* **2013**, *43*, 1–7. [[CrossRef](#)]
15. Means, J.E.; Acker, S.A.; Harding, D.J.; Blair, J.B.; Lefsky, M.A.; Cohen, W.B.; Harmon, M.E.; McKee, W.A. Use of large-footprint scanning airborne lidar to estimate forest stand characteristics in the Western Cascades of Oregon. *Remote Sens. Environ.* **1999**, *67*, 298–308. [[CrossRef](#)]
16. Watt, P.; Watt, M.S. Development of a national model of Pinus radiata stand volume from LiDAR metrics for New Zealand. *Int. J. Remote Sens.* **2013**, *34*, 5892–5904. [[CrossRef](#)]
17. Coops, N.C.; Hilker, T.; Wulder, M.A.; St-Onge, B.; Newnham, G.; Siggins, A.; Trofymow, J.T. Estimating canopy structure of Douglas-fir forest stands from discrete-return LiDAR. *Trees* **2007**, *21*, 295. [[CrossRef](#)]
18. Magnussen, S.; Renaud, J.P. Multidimensional scaling of first-return airborne laser echoes for prediction and model-assisted estimation of a distribution of tree stem diameters. *Ann. For. Sci.* **2016**, *73*, 1089–1098. [[CrossRef](#)]
19. Prieditis, G.; Šmits, I.; Arhipova, I.; Daģis, S.; Dubrovskis, D. Tree diameter models from field and remote sensing data. *Int. J. Math. Models Methods Appl. Sci.* **2012**, *6*, 707–714.

20. Tandoc, F.A.M.; Paringit, E.C.; Bantayan, N.C.; Argamosa, R.J.L.; Faelga, R.A.G.; Ibañez, C.A.G.; Posilero, M.A.V.; Zaragosa, G.P.; Malabanan, M.V. Diameter at breast height estimation in Mt. Makiling, Laguna, Philippines using metrics derived from airborne LiDAR data and Worldview-2 bands. In *Lidar Remote Sensing for Environmental Monitoring XV*; International Society for Optics and Photonics: Bellingham, WA, USA, 2016; p. 98791C.
21. Kato, A.; Moskal, L.M.; Schiess, P.; Swanson, M.E.; Calhoun, D.; Stuetzle, W. Capturing tree crown formation through implicit surface reconstruction using airborne lidar data. *Remote Sens. Environ.* **2009**, *113*, 1148–1162. [[CrossRef](#)]
22. Popescu, S.C.; Wynne, R.H.; Nelson, R.F. Measuring individual tree crown diameter with lidar and assessing its influence on estimating forest volume and biomass. *Can. J. Remote Sens.* **2003**, *29*, 564–577. [[CrossRef](#)]
23. Mikita, T.; Patočka, Z.; Sabol, J. Estimation of leaf area index (LAI) in forests on the basis of airborne laser scanning in the conditions of the Czech Republic. *Zpr. Lesn. Vyzk.* **2014**, *59*, 234–242.
24. Pearse, G.D.; Morgenroth, J.; Watt, M.S.; Dash, J.P. Optimising prediction of forest leaf area index from discrete airborne lidar. *Remote Sens. Environ.* **2017**, *200*, 220–239. [[CrossRef](#)]
25. Zhang, D.; Liu, J.; Ni, W.; Sun, G.; Zhang, Z.; Liu, Q.; Wang, Q. Estimation of Forest Leaf Area Index Using Height and Canopy Cover Information Extracted From Unmanned Aerial Vehicle Stereo Imagery. *IEEE J. Sel. Top. Appl. Earth Obs. Remote Sens.* **2019**, *12*, 471–481. [[CrossRef](#)]
26. Kaartinen, H.; Hyypä, J.; Yu, X.; Vastaranta, M.; Hyypä, H.; Kukko, A.; Holopainen, M.; Heipke, C.; Hirschmugl, M.; Morsdorf, F.; et al. An international comparison of individual tree detection and extraction using airborne laser scanning. *Remote Sens.* **2012**, *4*, 950–974. [[CrossRef](#)]
27. Eysn, L.; Hollaus, M.; Lindberg, E.; Berger, F.; Monnet, J.M.; Dalponte, M.; Kobal, M.; Pellegrini, M.; Lingua, E.; Mongus, D.; et al. A benchmark of lidar-based single tree detection methods using heterogeneous forest data from the Alpine Space. *Forests* **2015**, *6*, 1721–1747. [[CrossRef](#)]
28. Watt, M.S.; Meredith, A.; Watt, P.; Gunn, A. Use of LiDAR to estimate stand characteristics for thinning operations in young douglas-fir plantations. *N. Z. J. For. Sci.* **2013**, *43*, 1–10. [[CrossRef](#)]
29. Lang, M.; Arumäe, T. Assessment of forest thinning intensity using sparse point clouds from repeated airborne lidar measurements. *For. Stud.* **2018**, *68*, 40–50. [[CrossRef](#)]
30. González-Ferreiro, E.; Diéguez-Aranda, U.; Crecente-Campo, F.; Barreiro-Fernández, L.; Miranda, D.; Castedo-Dorado, F. Modelling canopy fuel variables for *Pinus radiata* D. Don in NW Spain with low-density LiDAR data. *Int. J. Wildland Fire* **2014**, *23*, 350–362. [[CrossRef](#)]
31. Fernández-álvarez, M.; Armesto, J.; Picos, J. LiDAR-based wildfire prevention in WUI: The automatic detection, measurement and evaluation of forest fuels. *Forests* **2019**, *10*, 148. [[CrossRef](#)]
32. Fidalgo-González, L.A.; Arellano-Pérez, S.; Álvarez-González, J.G.; Castedo-Dorado, F.; Ruiz-González, A.D.; González-Ferreiro, E. Estimation of the vertical distribution of the fine canopy fuel in *pinus sylvestris* stands using low density LiDAR data. *Rev. Teledetec.* **2019**, *2019*, 1–16. [[CrossRef](#)]
33. Hevia, A.; Álvarez-González, J.G.; Ruiz-Fernández, E.; Prendes, C.; Ruiz-González, A.D.; Majada, J.; González-Ferreiro, E. Modelling canopy fuel and forest stand variables and characterizing the influence of thinning in the stand structure using airborne LiDAR. *Rev. Teledetec.* **2016**, *2016*, 41–45. [[CrossRef](#)]
34. Ferraz, A.; Saatchi, S.; Mallet, C.; Jacquemoud, S.; Gonçalves, G.; Silva, C.A.; Soares, P.; Tomé, M.; Pereira, L. Airborne lidar estimation of aboveground forest biomass in the absence of field inventory. *Remote Sens.* **2016**, *8*, 653. [[CrossRef](#)]
35. Sheridan, R.D.; Popescu, S.C.; Gatzliolis, D.; Morgan, C.L.S.; Ku, N.W. Modeling forest aboveground biomass and volume using airborne LiDAR metrics and forest inventory and analysis data in the pacific northwest. *Remote Sens.* **2015**, *7*, 229–255. [[CrossRef](#)]
36. Rosette, J.; Suárez, J.; Nelson, R.; Los, S.; Cook, B.; North, P. Lidar remote sensing for biomass assessment. *Remote Sens. Biomass—Princ. Appl.* **2012**, *24*, 3–27.
37. Zolkos, S.G.; Goetz, S.J.; Dubayah, R. A meta-analysis of terrestrial aboveground biomass estimation using lidar remote sensing. *Remote Sens. Environ.* **2013**, *128*, 289–298. [[CrossRef](#)]
38. Popescu, S.C. Estimating biomass of individual pine trees using airborne lidar. *Biomass Bioenergy* **2007**, *31*, 646–655. [[CrossRef](#)]
39. Silva, C.A.; Klauber, C.E.; Carvalho, S.D.P.C.; Hudak, A.T.; Rodriguez, L.C.E. Mapping aboveground carbon stocks using LiDAR data in *Eucalyptus* spp. plantations in the state of São Paulo, Brazil. *Sci. For.* **2014**, *42*, 591–604.

40. Spriggs, R.A.; Vanderwel, M.C.; Jones, T.A.; Caspersen, J.P.; Coomes, D.A. A critique of general allometry-inspired models for estimating forest carbon density from airborne LiDAR. *PLoS ONE* **2019**, *14*, e0215238. [[CrossRef](#)]
41. Vincent, G.; Sabatier, D.; Rutishauser, E. Revisiting a universal airborne light detection and ranging approach for tropical forest carbon mapping: Scaling-up from tree to stand to landscape. *Oecologia* **2014**, *175*, 439–443. [[CrossRef](#)]
42. Andersen, H.-E.; Reutebuch, S.E.; McGaughey, R.J. A rigorous assessment of tree height measurements obtained using airborne lidar and conventional field methods. *Can. J. Remote Sens.* **2006**, *32*, 355–366. [[CrossRef](#)]
43. Xu, C.; Manley, B.; Morgenroth, J. Evaluation of modelling approaches in predicting forest volume and stand age for small-scale plantation forests in New Zealand with RapidEye and LiDAR. *Int. J. Appl. Earth Obs. Geoinf.* **2018**, *73*, 386–396. [[CrossRef](#)]
44. Holmgren, J.; Nilsson, M.; Olsson, H. Estimation of tree height and stem volume on plots using airborne laser scanning. *For. Sci.* **2003**, *49*, 419–428.
45. Næsset, E.; Bjerknes, K.-O. Estimating tree heights and number of stems in young forest stands using airborne laser scanner data. *Remote Sens. Environ.* **2001**, *78*, 328–340. [[CrossRef](#)]
46. Persson, A.; Holmgren, J.; Soderman, U. Detecting and measuring individual trees using an airborne laser scanner. *Photogramm. Eng. Remote Sens.* **2002**, *68*, 925–932.
47. Liang, X.; Wang, Y.; Pyörälä, J.; Lehtomäki, M.; Yu, X.; Kaartinen, H.; Kukko, A.; Honkavaara, E.; Issaoui, A.E.I.; Nevalainen, O.; et al. Forest in situ observations using unmanned aerial vehicle as an alternative of terrestrial measurements. *For. Ecosyst.* **2019**, *6*, 20. [[CrossRef](#)]
48. Wang, Y.; Hyyppä, J.; Liang, X.; Kaartinen, H.; Yu, X.; Lindberg, E.; Holmgren, J.; Qin, Y.; Mallet, C.; Ferraz, A. International benchmarking of the individual tree detection methods for modeling 3-D canopy structure for silviculture and forest ecology using airborne laser scanning. *IEEE Trans. Geosci. Remote Sens.* **2016**, *54*, 5011–5027. [[CrossRef](#)]
49. Jaakkola, A.; Hyyppä, J.; Kukko, A.; Yu, X.; Kaartinen, H.; Lehtomäki, M.; Lin, Y. A low-cost multi-sensoral mobile mapping system and its feasibility for tree measurements. *ISPRS J. Photogramm. Remote Sens.* **2010**, *65*, 514–522. [[CrossRef](#)]
50. Wallace, L.; Lucieer, A.; Watson, C.; Turner, D. Development of a UAV-LiDAR system with application to forest inventory. *Remote Sens.* **2012**, *4*, 1519–1543. [[CrossRef](#)]
51. Cao, L.; Liu, H.; Fu, X.; Zhang, Z.; Shen, X.; Ruan, H. Comparison of UAV LiDAR and digital aerial photogrammetry point clouds for estimating forest structural attributes in subtropical planted forests. *Forests* **2019**, *10*, 145. [[CrossRef](#)]
52. Jaakkola, A.; Hyyppä, J.; Yu, X.; Kukko, A.; Kaartinen, H.; Liang, X.; Hyyppä, H.; Wang, Y. Autonomous collection of forest field reference—The outlook and a first step with UAV laser scanning. *Remote Sens.* **2017**, *9*, 785. [[CrossRef](#)]
53. Puliti, S.; Dash, J.P.; Watt, M.S.; Breidenbach, J.; Pearse, G.D. A comparison of UAV laser scanning, photogrammetry and airborne laser scanning for precision inventory of small-forest properties. *For. Int. J. For. Res.* **2020**, *93*, 150–162. [[CrossRef](#)]
54. Sankey, T.; Donager, J.; McVay, J.; Sankey, J.B. UAV lidar and hyperspectral fusion for forest monitoring in the southwestern USA. *Remote Sens. Environ.* **2017**, *195*, 30–43. [[CrossRef](#)]
55. Li, J.; Yang, B.; Cong, Y.; Cao, L.; Fu, X.; Dong, Z. 3D Forest Mapping Using A Low-Cost UAV Laser Scanning System: Investigation and Comparison. *Remote Sens.* **2019**, *11*, 717. [[CrossRef](#)]
56. Brede, B.; Lau, A.; Bartholomeus, H.M.; Kooistra, L. Comparing RIEGL RiCOPTER UAV LiDAR derived canopy height and DBH with terrestrial LiDAR. *Sensors* **2017**, *17*, 2371. [[CrossRef](#)]
57. Wallace, L.; Musk, R.; Lucieer, A. An assessment of the repeatability of automatic forest inventory metrics derived from UAV-borne laser scanning data. *IEEE Trans. Geosci. Remote Sens.* **2014**, *52*, 7160–7169. [[CrossRef](#)]
58. Iglhaut, J.; Cabo, C.; Puliti, S.; Piermattei, L.; O'Connor, J.; Rosette, J. Structure from Motion Photogrammetry in Forestry: A Review. *Curr. For. Rep.* **2019**, *5*, 155–168. [[CrossRef](#)]
59. Birdal, A.C.; Avdan, U.; Türk, T. Estimating tree heights with images from an unmanned aerial vehicle. *Geomat. Nat. Hazards Risk* **2017**, *8*, 1144–1156. [[CrossRef](#)]

60. Fankhauser, K.E.; Strigul, N.S.; Gatzliolis, D. Augmentation of traditional forest inventory and Airborne laser scanning with unmanned aerial systems and photogrammetry for forest monitoring. *Remote Sens.* **2018**, *10*, 1562. [[CrossRef](#)]
61. Frey, J.; Kovach, K.; Stemmler, S.; Koch, B. UAV photogrammetry of forests as a vulnerable process. A sensitivity analysis for a structure from motion RGB-image pipeline. *Remote Sens.* **2018**, *10*, 912. [[CrossRef](#)]
62. Guerra-Hernández, J.; González-Ferreiro, E.; Monleón, V.J.; Faias, S.P.; Tomé, M.; Díaz-Varela, R.A. Use of multi-temporal UAV-derived imagery for estimating individual tree growth in *Pinus pinea* stands. *Forests* **2017**, *8*, 300. [[CrossRef](#)]
63. Hentz, Â.M.K.; Silva, C.A.; Dalla Corte, A.P.; Netto, S.P.; Strager, M.P.; Klauberg, C. Estimating forest uniformity in *Eucalyptus* spp. and *Pinus taeda* L. stands using field measurements and structure from motion point clouds generated from unmanned aerial vehicle (UAV) data collection. *For. Syst.* **2018**, *27*, e005. [[CrossRef](#)]
64. Iizuka, K.; Yonehara, T.; Itoh, M.; Kosugi, Y. Estimating Tree Height and Diameter at Breast Height (DBH) from Digital surface models and orthophotos obtained with an unmanned aerial system for a Japanese Cypress (*Chamaecyparis obtusa*) Forest. *Remote Sens.* **2018**, *10*, 13. [[CrossRef](#)]
65. Krause, S.; Sanders, T.G.M.; Mund, J.P.; Greve, K. UAV-based photogrammetric tree height measurement for intensive forest monitoring. *Remote Sens.* **2019**, *11*, 758. [[CrossRef](#)]
66. Moukomla, S.; Srestasathien, P.; Siripon, S.; Wasuhiranyrith, R.; Kooha, P. Estimating above ground biomass for eucalyptus plantation using data from unmanned aerial vehicle imagery. *Remote Sens. Agric. Ecosyst. Hydrol.* **XX** **2018**, 1078308. [[CrossRef](#)]
67. Dempewolf, J.; Nagol, J.; Hein, S.; Thiel, C.; Zimmermann, R. Measurement of within-season tree height growth in a mixed forest stand using UAV imagery. *Forests* **2017**, *8*, 231. [[CrossRef](#)]
68. Fraser, B.T.; Congalton, R.G. Issues in Unmanned Aerial Systems (UAS) data collection of complex forest environments. *Remote Sens.* **2018**, *10*, 908. [[CrossRef](#)]
69. Ota, T.; Ogawa, M.; Mizoue, N.; Fukumoto, K.; Yoshida, S. Forest Structure Estimation from a UAV-Based Photogrammetric Point Cloud in Managed Temperate Coniferous Forests. *Forests* **2017**, *8*, 343. [[CrossRef](#)]
70. Panagiotidis, D.; Abdollahnejad, A.; Surový, P.; Chiteculo, V. Determining tree height and crown diameter from high-resolution UAV imagery. *Int. J. Remote Sens.* **2017**, *38*, 2392–2410. [[CrossRef](#)]
71. Puliti, S.; Ørka, H.O.; Gobakken, T.; Næsset, E. Inventory of small forest areas using an unmanned aerial system. *Remote Sens.* **2015**, *7*, 9632–9654. [[CrossRef](#)]
72. Thiel, C.; Schmulilius, C. Derivation of forest parameters from stereographic UAV data—A comparison with airborne lidar data. In Proceedings of the Living Planet Symposium, Prague, Czech Republic, 9–13 May 2016.
73. Balenović, I.; Marjanović, H. Selection of the optimal spatial resolution of image-based digital surface models for use in forestry—Example from the area of Lowland oak forests. *Nova Meh. Šumar.* **2016**, *37*, 1–13.
74. Dandois, J.P.; Ellis, E.C. High spatial resolution three-dimensional mapping of vegetation spectral dynamics using computer vision. *Remote Sens. Environ.* **2013**, *136*, 259–276. [[CrossRef](#)]
75. Dandois, J.P.; Olano, M.; Ellis, E.C. Optimal altitude, overlap, and weather conditions for computer vision uav estimates of forest structure. *Remote Sens.* **2015**, *7*, 13895–13920. [[CrossRef](#)]
76. Lisein, J.; Bonnet, S.; Lejeune, P.; Pierrot-Deseilligny, M. Modeling of the forest canopy by photogrammetry from the images acquired by drone. *Rev. Fr. Photogramm. Teledetect.* **2014**, *206*, 45–54.
77. Lisein, J.; Pierrot-Deseilligny, M.; Bonnet, S.; Lejeune, P. A photogrammetric workflow for the creation of a forest canopy height model from small unmanned aerial system imagery. *Forests* **2013**, *4*, 922–944. [[CrossRef](#)]
78. Moe, K.T.; Owari, T.; Furuya, N.; Hiroshima, T. Comparing Individual Tree Height Information Derived from Field Surveys, LiDAR and UAV-DAP for High-Value Timber Species in Northern Japan. *Forests* **2020**, *11*, 223. [[CrossRef](#)]
79. Alonzo, M.; Andersen, H.E.; Morton, D.C.; Cook, B.D. Quantifying boreal forest structure and composition using UAV structure from motion. *Forests* **2018**, *9*, 119. [[CrossRef](#)]
80. Ni, W.; Liu, J.; Zhang, Z.; Sun, G.; Yang, A. Evaluation of UAV-based forest inventory system compared with LiDAR data. In Proceedings of the 2015 IEEE International Geoscience and Remote Sensing Symposium (IGARSS), Milano, Italy, 26–31 July 2015; pp. 3874–3877.

81. Ni, W.; Sun, G.; Pang, Y.; Zhang, Z.; Liu, J.; Yang, A.; Wang, Y.; Zhang, D. Mapping Three-Dimensional Structures of Forest Canopy Using UAV Stereo Imagery: Evaluating Impacts of Forward Overlaps and Image Resolutions with LiDAR Data as Reference. *IEEE J. Sel. Top. Appl. Earth Obs. Remote Sens.* **2018**, *11*, 3578–3589. [[CrossRef](#)]
82. Reuben, J.; Hussin, Y.; Kloosterman, H.; Ismail, M.H. Tree height derived from point clouds of UAV compared to airborne laser scanning and its effect on estimating biomass and carbon stock in tropical rain forest of Malaysia. In Proceedings of the 38th Asian Conference on Remote Sensing—Space Applications: Touching Human Lives, ACRS 2017, New Delhi, India, 23–27 October 2017.
83. Huang, H.; He, S.; Chen, C. Leaf abundance affects tree height estimation derived from UAV images. *Forests* **2019**, *10*, 931. [[CrossRef](#)]
84. Yurtseven, H.; Akgul, M.; Coban, S.; Gulci, S. Determination and accuracy analysis of individual tree crown parameters using UAV based imagery and OBIA techniques. *Meas. J. Int. Meas. Confed.* **2019**, *145*, 651–664. [[CrossRef](#)]
85. Fawcett, D.; Azlan, B.; Hill, T.C.; Kho, L.K.; Bennie, J.; Anderson, K. Unmanned aerial vehicle (UAV) derived structure-from-motion photogrammetry point clouds for oil palm (*Elaeis guineensis*) canopy segmentation and height estimation. *Int. J. Remote Sens.* **2019**, *40*, 7538–7560. [[CrossRef](#)]
86. Zainuddin, K.; Jaffri, M.H.; Zainal, M.Z.; Ghazali, N.; Samad, A.M. Verification test on ability to use low-cost UAV for quantifying tree height. In Proceedings of the 2016 IEEE 12th International Colloquium on Signal Processing & Its Applications (CSPA), Melaka, Malaysia, 4–6 March 2016; pp. 317–321.
87. Shin, P.; Sankey, T.; Moore, M.; Thode, A. Evaluating unmanned aerial vehicle images for estimating forest canopy fuels in a ponderosa pine stand. *Remote Sens.* **2018**, *10*, 1266. [[CrossRef](#)]
88. Karpina, M.; Jarzabek-Rychard, M.; Tymków, P.; Borkowski, A. UAV-based automatic tree growth measurement for biomass estimation. *Int. Arch. Photogramm. Remote Sens. Spat. Inf. Sci.* **2016**, *8*, 685–688. [[CrossRef](#)]
89. Jayathunga, S.; Owari, T.; Tsuyuki, S.; Hirata, Y. Potential of UAV photogrammetry for characterization of forest canopy structure in uneven-aged mixed conifer–broadleaf forests. *Int. J. Remote Sens.* **2020**, *41*, 53–73. [[CrossRef](#)]
90. Wallace, L.; Lucieer, A.; Malenovsky, Z.; Turner, D.; Vopěnka, P. Assessment of forest structure using two UAV techniques: A comparison of airborne laser scanning and structure from motion (SfM) point clouds. *Forests* **2016**, *7*, 62. [[CrossRef](#)]
91. Hall, P. *Mechanical Site Preparation Survey*; New Zealand Forest Site Management Cooperative: Rotorua, New Zealand, 1996; pp. 1–17.
92. Paterson, D.B.; Mason, W.L. *Cultivation of Soils for Forestry*; Forestry Commission Bulletin: London, UK, 1999.
93. Pix4D. Step 1. Before Starting a Project > 4. Getting GCPs on the Field or through other Sources (Optional but Recommended). Available online: <https://support.pix4d.com/hc/en-us/articles/202557489-Step-1-Before-Starting-a-Project-4-Getting-GCPs-on-the-field-or-through-other-sources-optional-but-recommended> (accessed on 5 March 2020).
94. Hartley, R.; Melia, N.; Estarija, H.J.; Watt, M.S.; Pearce, G.; Massam, P.; Wright, L.A.H.; Stovold, G.T. *An Assessment of UAV Laser Scanning and Photogrammetric Point Clouds for the Measurement of Young Forestry Trials*; Scion, Growing Confidence in Forestry’s Future Technical Note GCFF TN-028: Rotorua, New Zealand, 2019; pp. 1–11.
95. Pix4D. Support Pix4Dmapper Manual: Menu Process > Processing Options... > 1. Initial Processing > Matching. Available online: <https://support.pix4d.com/hc/en-us/articles/205433155-Menu-Process-Processing-Options-1-Initial-Processing-Matching> (accessed on 17 June 2020).
96. Esri Inc. *ArcGIS Pro, Version 2.5.1*; Esri Inc.: Redlands, CA, USA, 2019.
97. Isenburg, M. *LAStools—Efficient LiDAR Processing Software*; Rapidlasso GmbH: Gilching, Germany, 2019.
98. Roussel, J.-R.; Auty, D.; De Boissieu, F.; Meador, A. lidR: Airborne LiDAR data manipulation and visualization for forestry applications. *R Package Version* **2018**, *1*.
99. R Core Team. *R: A Language and Environment for Statistical Computing*; R Foundation for Statistical Computing: Vienna, Austria, 2020.
100. Girardeau-Montaut, D. CloudCompare; Version 2.1.1. 2020. Available online: <http://cloudcompare.org/> (accessed on 2 June 2020).

101. Dash, J.P.; Watt, M.S.; Hartley, R.J.L. *Testing UAV-Borne Riegl Mini VUX-1 Scanner for Phenotyping a Mature Genetics Trial*; Scion, Growing Confidence in Forestry's Future Technical Note GCFF TN-023: Rotorua, New Zealand, 2019; pp. 1–9.
102. Hyypä, J.; Hyypä, H.; Litkey, P.; Yu, X.; Haggrén, H.; Rönnholm, P.; Pyysalo, U.; Pitkänen, J.; Maltamo, M. Algorithms and methods of airborne laser scanning for forest measurements. *Int. Arch. Photogramm. Remote Sens. Spat. Inf. Sci.* **2004**, *36*, 82–89.
103. Aldred, A.H.; Bonnor, G.M. *Application of Airborne Lasers to Forest Surveys*; Information Report PI-X-051; Agriculture Canada, Ministry of State for Forestry, Petawawa National Forestry Institute: Chalk River, ON, Canada, 1985; 62p.
104. Hyypä, J. Detecting and estimating attributes for single trees using laser scanner. *Photogramm. J. Finl.* **1999**, *16*, 27–42.
105. Korpela, I.; Dahlin, B.; Schäfer, H.; Bruun, E.; Haapaniemi, F.; Honkasalo, J.; Ilvesniemi, S.; Kuutti, V.; Linkosalmi, M.; Mustonen, J. Single-tree forest inventory using lidar and aerial images for 3D treetop positioning, species recognition, height and crown width estimation. In Proceedings of the ISPRS workshop on laser scanning, Enschede, The Netherlands, 12–13 June 2019; pp. 227–233.
106. Roussel, J.R.; Caspersen, J.; Béland, M.; Thomas, S.; Achim, A. Removing bias from LiDAR-based estimates of canopy height: Accounting for the effects of pulse density and footprint size. *Remote Sens. Environ.* **2017**, *198*, 1–16. [[CrossRef](#)]
107. Riegl. RIEGL miniVUX-1UAV Datasheet. Available online: http://www.riegl.com/uploads/tx_pxpriegldownloads/RIEGL_miniVUX-1UAV_Datasheet_2020-03-31.pdf (accessed on 2 June 2020).
108. Schaer, P.; Skaloud, J.; Landtwin, S.; Legat, K. Accuracy estimation for laser point cloud including scanning geometry. In Proceedings of the Mobile Mapping Symposium 2007, Padova, Italy, 29–31 May 2007.
109. Brieger, F.; Herzsuh, U.; Pestryakova, L.A.; Bookhagen, B.; Zakharov, E.S.; Kruse, S. Advances in the derivation of Northeast Siberian forest metrics using high-resolution UAV-based photogrammetric point clouds. *Remote Sens.* **2019**, *11*, 1447. [[CrossRef](#)]
110. Lin, J.; Wang, M.; Ma, M.; Lin, Y. Aboveground tree biomass estimation of sparse subalpine coniferous forest with UAV oblique photography. *Remote Sens.* **2018**, *10*, 1849. [[CrossRef](#)]
111. Surový, P.; Almeida Ribeiro, N.; Panagiotidis, D. Estimation of positions and heights from UAV-sensed imagery in tree plantations in agrosilvopastoral systems. *Int. J. Remote Sens.* **2018**, *39*, 4786–4800. [[CrossRef](#)]
112. O'Connor, J.; Smith, M.J.; James, M.R. Cameras and settings for aerial surveys in the geosciences: Optimising image data. *Prog. Phys. Geogr.* **2017**, *41*, 325–344. [[CrossRef](#)]
113. Osborn, J.; Dell, M.; Stone, C.; Iqbal, I.; Lacey, M.; Lucieer, A.; McCoull, C. Photogrammetry for forest inventory: Planning Guidelines. 2017. Available online: https://www.fwpa.com.au/images/resources/2017/Photogrammetry_for_Forest_Inventory_Planning_Guide_PNC326-1314.pdf (accessed on 5 June 2020).
114. DJI Ltd. Phantom 4 Pro V2.0 Specs. Available online: <https://www.dji.com/nz/phantom-4-pro-v2/specs> (accessed on 5 June 2020).
115. Pádua, L.; Marques, P.; Adão, T.; Hruška, J.; Peres, E.; Morais, R.; Sousa, A.; Sousa, J.J. UAS-based imagery and photogrammetric processing for tree height and crown diameter extraction. In Proceedings of the International Conference on Geoinformatics and Data Analysis, Prague, Czech Republic, 20–22 April 2018; pp. 87–91.
116. Goldbergs, G.; Maier, S.W.; Levick, S.R.; Edwards, A. Efficiency of individual tree detection approaches based on light-weight and low-cost UAS imagery in Australian Savannas. *Remote Sens.* **2018**, *10*, 161. [[CrossRef](#)]
117. Zahawi, R.A.; Dandois, J.P.; Holl, K.D.; Nadwodny, D.; Reid, J.L.; Ellis, E.C. Using lightweight unmanned aerial vehicles to monitor tropical forest recovery. *Biol. Conserv.* **2015**, *186*, 287–295. [[CrossRef](#)]
118. Kellner, J.R.; Armston, J.; Birrer, M.; Cushman, K.; Duncanson, L.; Eck, C.; Fallegger, C.; Imbach, B.; Král, K.; Krůček, M. New opportunities for forest remote sensing through ultra-high-density drone lidar. *Surv. Geophys.* **2019**, *40*, 959–977. [[CrossRef](#)]

Publisher's Note: MDPI stays neutral with regard to jurisdictional claims in published maps and institutional affiliations.



© 2020 by the authors. Licensee MDPI, Basel, Switzerland. This article is an open access article distributed under the terms and conditions of the Creative Commons Attribution (CC BY) license (<http://creativecommons.org/licenses/by/4.0/>).